RESEARCH ARTICLE | OCTOBER 06 2023

Proof of concept: Real-time flux density monitoring system on external tube receivers for optimized solar field operation

Christian Raeder ✉; Matthias Offergeld; Marc Röger; Alexander Lademann; Judith Zöller; Matthias Glinka; José Escamilla; Andreas Kämpgen

AIP Conf. Proc. 2815, 080008 (2023)
https://doi.org/10.1063/5.0148725

Proof of Concept: Real-Time Flux Density Monitoring System on External Tube Receivers for Optimized Solar Field Operation

Christian Raeder[1,a)], Matthias Offergeld[1], Marc Röger[2], Alexander Lademann[1], Judith Zöller[1], Matthias Glinka[1], José Escamilla[3], and Andreas Kämpgen[3]

[1]*German Aerospace Center (DLR), Institute of Solar Research, Professor-Rehm-Straße 1, 52428 Jülich, Germany*
[2]*German Aerospace Center (DLR), Institute of Solar Research, Paseo de Almeria 73, 04001 Almería, Spain*
[3]*CSP Services España, S.L., Paseo de Almería, 73, 04001 Almería, Spain*

[a)] Corresponding author: Christian.raeder@dlr.de

Abstract. An experimental tube receiver was constructed, built and brought to operation. This receiver served as a model to try out the so-called scan-method and the measurement of the flux density by reflection off the receiver in real time during irradiation. A comparison with a flux map obtained by a radiometer-based method shows qualitatively similar results. It is concluded that the camera-method is applicable to tube receivers. Experiments at large-scale industrial receivers are planned.

INTRODUCTION

To determine the efficiency of a heliostat field and a solar receiver separately, as well as the monitoring of the receiver operation, it is essential to know the exact amount of incident flux. Ideally at any given time. The usage of moving bars on large scale receivers for this purpose has several disadvantages: the incident flux will be shadowed off the receiver during the measurement process, the installation on large scale receivers causes a high hardware expenditure and is technically difficult to implement. To face this issue a flux density measurement system on open volumetric receivers was introduced by M. Röger et al [1]: By recording the reflection off the receiver with a digital camera, combined with the knowledge of the bidirectional reflection distribution function (BRDF), it is possible to estimate the incident flux. F. Göhring et al [2] obtained the BRDF by measuring the single absorber cups in a gonioreflectometer (GoRef). M. Offergeld et al [3] showed an in-situ method to determine the BRDF of a volumetric receiver with the so-called scan method. The advantages are clearly convincing: a low hardware expenditure, whilst only a camera and software is needed, the operation of the solar power plant is not disturbed and the measurement time is a matter of seconds.

In this article the transition of the scan method to determine the BRDF is put forward to external tube receivers and first results of the measured flux density on such receivers are presented.

EXPERIMENTAL TUBE RECEIVER

The experimental tube receiver (test receiver) was used exclusively for measuring the flux density and so the generated heat does not have to be used. 16 absorber tubes were used, with a distance of 1 mm from one another. The tubes of the test receiver are cooled with tap water. It has a temperature of about 15°C. The cooling is monitored by measuring the temperature of the inflowing water and by measuring the heated water flowing out. In addition, the mass flow of the cooling water is measured at one point.

SolarPACES: Solar Power & Chemical Energy Systems
AIP Conf. Proc. 2815, 080008-1–080008-9; https://doi.org/10.1063/5.0148725
Published by AIP Publishing. 978-0-7354-4623-6/$30.00

Eight radiometers are installed around the tube bundle (see Fig. 2). These have two functions when measuring the radiant flux density. On the one hand, they serve as a second measuring method to check the flux density measurement by means of reflection off the absorber. On the other hand, when measuring the flux density due to the reflections occurring at the absorber, calibration must take place, since only relative flux density values are measured initially. The cooling of the radiometers is provided by a 16 kW liquid cooler with a closed loop. The incoming water temperature is measured with a thermocouple, while each radiometer has a thermocouple to measure the outcoming water temperature. Furthermore, each cooling line for the radiometers is equipped with a flow switch to ensure proper cooling. Fig. 1 shows the piping and instrumentation diagram of the test receiver.

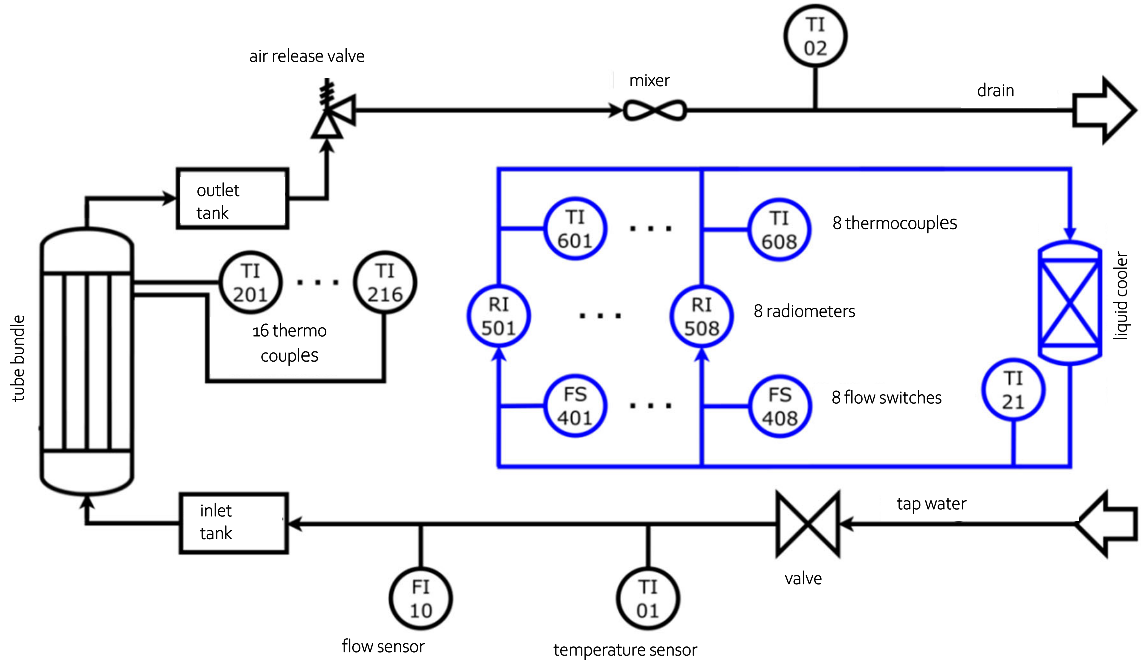

FIGURE 1. Piping and instrumentation diagram of the test receiver. Radiometer circuit in blue.

Stainless steel 1.4828 was selected as the material for the receiver tubes. The selected receiver tubes have an outer diameter of 42.4 mm with a wall thickness of 2.5 mm. Their length is 2385 mm, whereby the vertical part of the pipes is 1325 mm long. The receiver tubes are provided with a coating manufactured by BrightSource Energy, Israel and heat-treated at up to 600 °C. Fig. 2 (a) shows the CAD model of the receiver, (b) shows the readily prepared actual test receiver.

The solar radiation that hits the test receiver next to and between the receiver tubes must not penetrate into the test room. The integrated radiation shield reflects this radiation to the greatest possible extent diffusely. The material consists of two sheets of vacuum-pressed aluminum silicate wool (ASW). These panels are glued together and coated on the outside with an additional ASW coating, which makes them weatherproof and less hazardous to health. Behind the ASW panels is a flexible ASW layer, to compensate for different thermal expansions. This ASW structure is connected to the supporting metal back plate via a clamp connection.

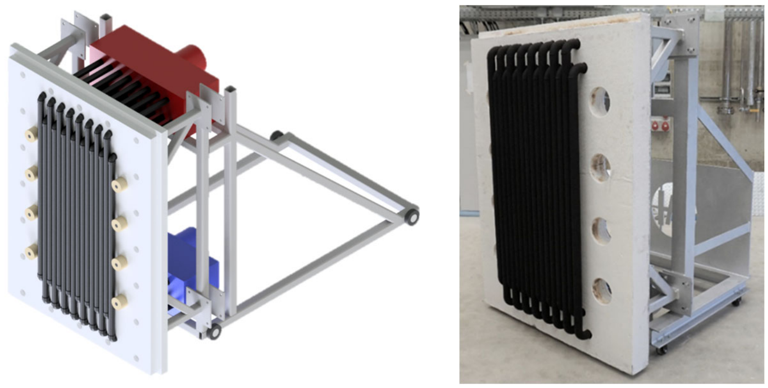

(a) (b)

FIGURE 2. (a) CAD model of the test receiver with steel construction, inlet- and outlet tank, radiation shield and radiometer setup. (b) A photo of the constructed receiver.

To the left and right of the test receiver, eight radiometers are evenly distributed around the tube bundle. These radiometers should be placed as close to the tube bundle as possible. For this aim, so-called radiometer sockets (see Fig 3.) were made of ASW, which are to serve the following purposes:

- Fixation of the radiometer
- Positioning of the radiometer close to the tube bundle with measuring surface in the plane tangent to the front of the tubes
- Non-destructive assembly and disassembly of socket and radiometer

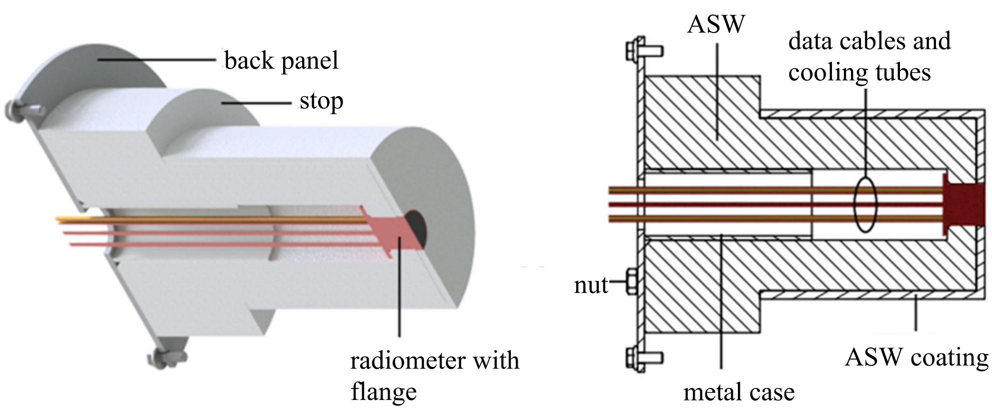

(a) (b)

FIGURE 3. Radiometer socket with radiometer in half section as CAD model (a) and as technical drawing (b).

Finally, the test receiver was installed on the first level of the multi focal tower of the German Aerospace Center, Jülich. Fig. 4 shows the setup.

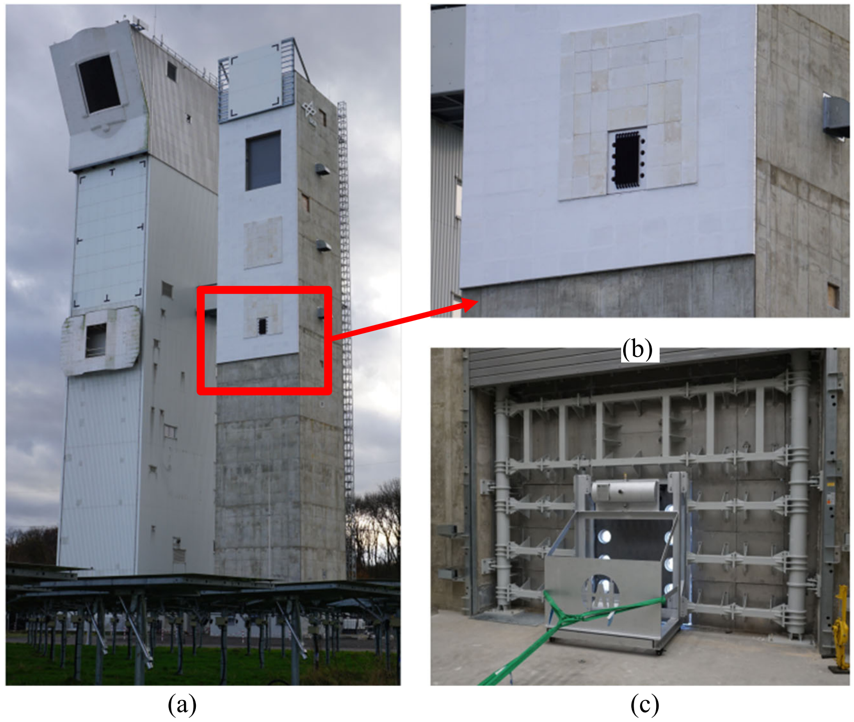

FIGURE 4. Installed test receiver, seen from outside ((a) and (b)) and from inside (c).

PRINCIPLE OF MEASUREMENT

The measurement method was previously described [3], [4]. In short, the method is divided into the scanning phase and a following measurement phase. In the scanning phase, the reflective properties (BDRF) of the external receiver surface is characterized by subsequently illuminating the receiver either by a single heliostat during sunshine or by a spotlight at night, while an image series is captured and afterwards merged into one single resulting image with (virtual) homogenous irradiation. During the measurement phase a digital camera captures images of the irradiated receiver. A radiometer mounted into the receiver surface (or nearby) calibrates the image grey values to solar flux density values. Taking scan results, directional composition and calibration into account, a software can calculate the solar fluxes using the radiation reflected off the receiver during the measurement phase.

Scan Method

Fig. 5 shows schematically the meander-shaped path of the light spot. During this scan process the camera, placed in front of the receiver, takes a high frequency (17 frames per second) series of images in order to get the maximum

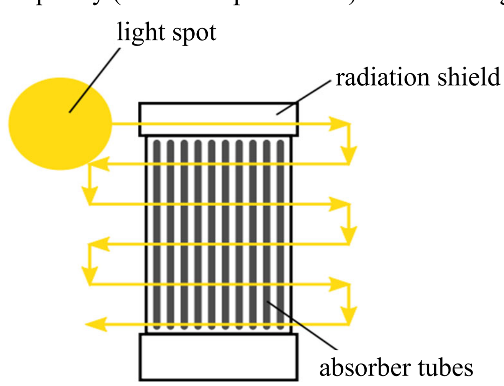

FIGURE 5. Schematic of the meandering path of the light spot on the absorber (scan).

image. Then we get the resulting correction matrices by applying the reciprocal values of all elements of the scan result. Fig. 6 shows the heliostat and camera positions at the Juelich Multifocal Tower (MFT). With the scan results from each direction (1 to 16) we obtain the BRDF of the receiver with the camera just in front of the MFT. As this project is work in progress we evaluated the data shown here with the scan result from position 10. Considering the application of the maximum image of a group 10 heliostat scan to an irradiation exposure from heliostats from the same group, the correction seems to work well (Fig. 9 (b)). In order to check whether this also applies to other heliostat field groups, the application of the scan result to a single image of the scan image series for groups 10, 11 and 12 is compared. In the result of group 10, stripes are only partially and easily recognizable. In the central area of the focal spot, there are hardly any stripes left after the scan result has been corrected. In the result image of group 11, the stripes can be seen more clearly. In the group 12 result, they are prominent. The cause of this abnormality could not be identified conclusively. The mutual shading of the tubes, which results from the increasing angle of incidence, is not a plausible reason for this. This should occur equally with the scan result and the radiation exposure and should therefore be considered in the correction. The observed phenomenon may be related to the fact that the absorber surface is currently described as a flat surface in the software and the pipe curvature is not considered. In order to obtain a more even result, the absorber surface was divided into 28 by 16 segments. The width of the individual segments corresponds to a tube width. The gray values of the pixels within a segment are averaged. For a higher resolution of the flux density distribution, an interpolation between the segments is then carried out.

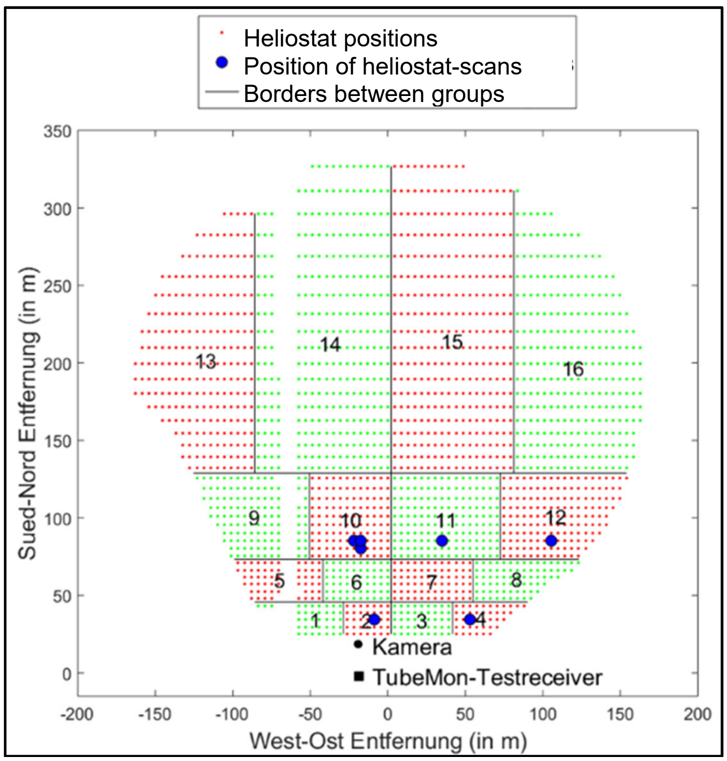

FIGURE 6. Grouping the heliostat field of the MFT/STJ in 16 groups. Data in this paper was evaluated with scans from group 10, 11 and 12.

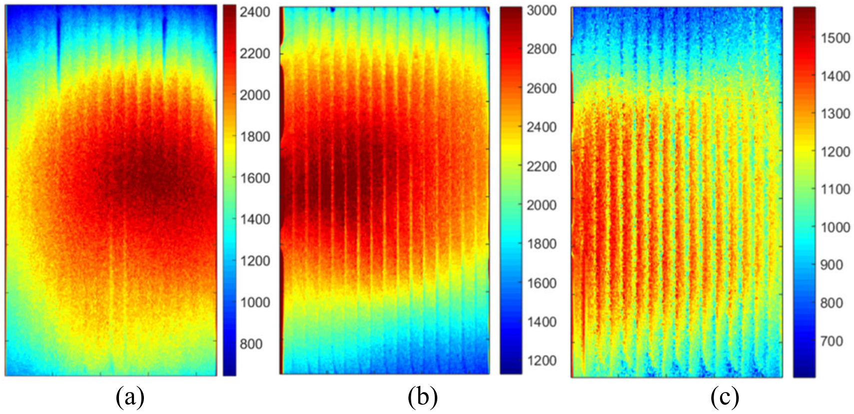

FIGURE 7. Application of the scan result to a single image out of the scan image series for (a) group 10, (b) group 11 and (c) group 12, scale as gray values.

A raw image was taken of the receiver surface, see Fig. 8 (a). This image was obtained when irradiated with 8 heliostats of group 10. This image is rectified and the gray values are transformed into false colors (Fig. 8 (b)). To make the further image processing easier we averaged the image segment by segment to have one-pixel column for each tube (Fig. 8 (c)). In the next step the image is corrected with the scan data (Fig. 9 (a)) and then interpolated to have smoother transitions. The focal spot is clearly visible and the maximum incident flux of around 15 kW/m² is plausible. As these were the very first experiments we only used a few heliostats to be safe from overheating the receiver. We only had surface temperatures just over 100 °C here. IR filters can be used at higher temperatures. Comparatively low camera sensitivity alone leads to a rather small influence.

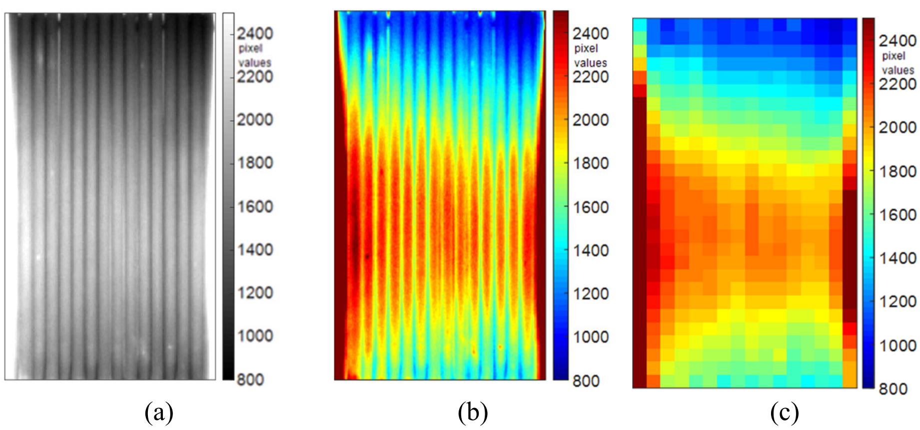

FIGURE 8. (a) raw image, (b) raw image, rectified, false colors, (c) segment wise averaged image.

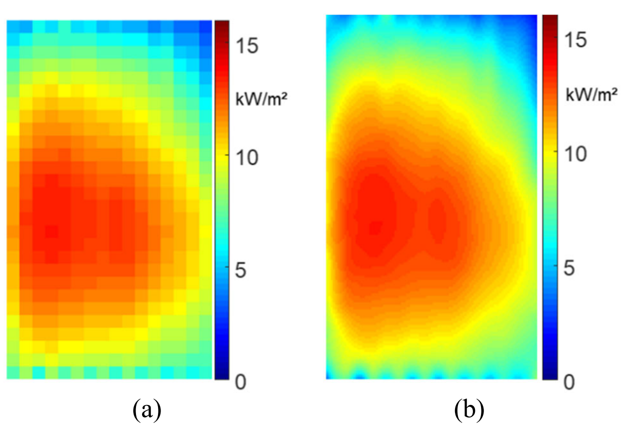

FIGURE 9. (a) corrected image, (b) corrected and interpolated image.

Radiometer Method – Focus Shift

The focus shift describes a method in which the beam focus is moved by several partial shifts over the radiometers. By lingering at the respective positions, we obtain a set of radiometer values during a reasonable amount of time (about 20 sec), an example is shown in Fig. 10. Recognizable plateaus can be seen in the curves of the radiometer readings over time. The start and end times of the plateaus are determined on the basis of these measurement curves and transferred to a MATLAB script. The measured values are then saved and the plateaus are averaged by the script and transferred into a matrix that gives each radiometer a flux density value for each step of the focus shift performed. By evaluating this matrix, the radiometer readings can be checked and the flux density distribution recorded can be interpolated into a flux map image.

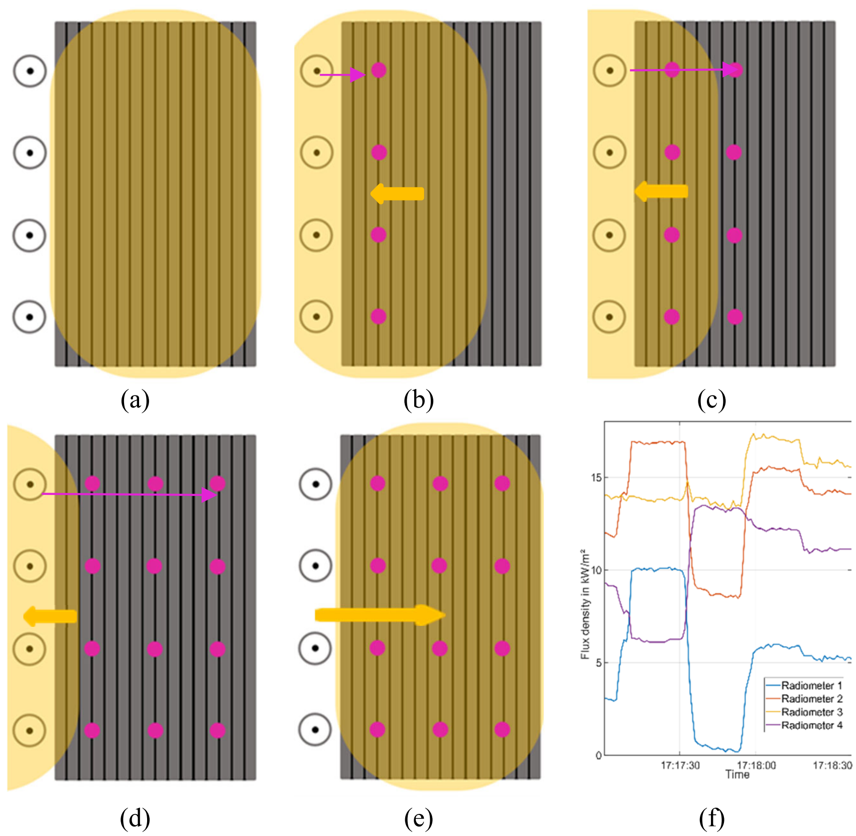

FIGURE 10. (a) Sketch of the tube receiver with the focal spot centered and the 4 radiometers on the left side. (b) the focal spot shifted to the left and in red the corresponding spots representing the measured values of the radiometers. (c) and (d) analogue to step (b) respectively, (e) the focal spot centered again on the receiver and (f) extract from measured values of the radiometer during the focus shift.

The flux map determined by the radiometer method is shown in Fig. 11 (a). The focal spot is clearly visible and the flux density of around 15 kW/m² in the center of the focal spot is reasonable. Fig. 11 (c) and (d) show the same for a maximum incident flux of about 28 kW/m² (24 Heliostat of groups 10, 11 and 12).

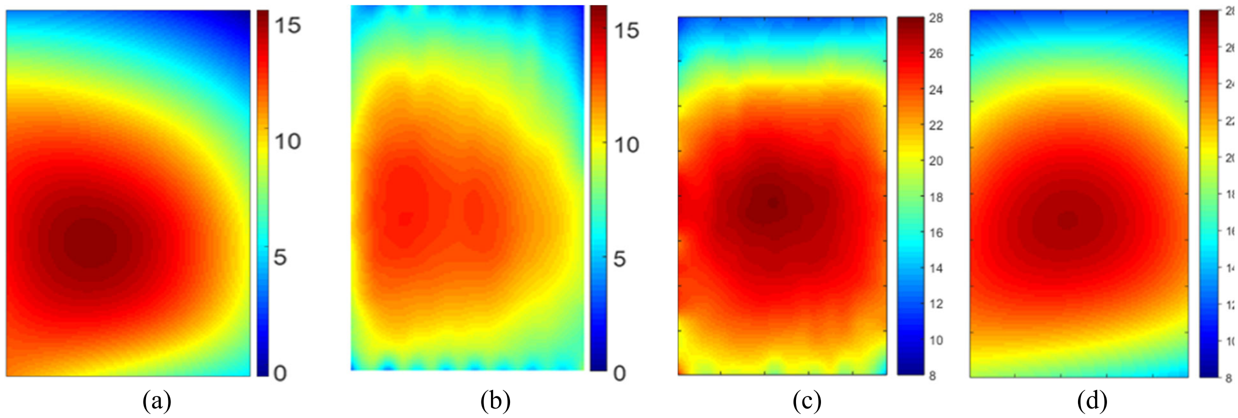

FIGURE 11. (a) Flux density distribution using Radiometer measurement and focus shift and (b) the flux map image obtained by reflection off the receiver to compare. Scan with Heliostat from position 10 (same as Fig. 9 (b)). (c) Flux density distribution using focus shift at higher incident flux. (d) flux map image obtained by reflection off the receiver at higher incident flux, corrected with heliostat-scans from position 10, 11 and 12.

The relative difference between camera-based and radiometer-based results are shown in Fig. 12.

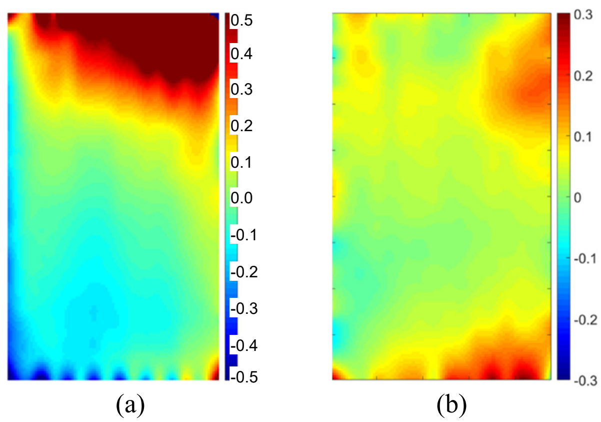

FIGURE 12. (a) Relative difference between images shown in Fig. 11 (a) and (b) and (b) relative difference between images shown in Fig. 11 (c) and (d).

RESULTS

The measurements of the flux distribution with the camera-method compared with the obtained values of the radiometer method show similar results in the distribution of the flux on the receiver. The results show that the determination of the incident flux by measuring the reflection off the receiver (camera-method) is applicable to tube receivers. Furthermore, when integrating the incident flux over the receiver surface the total flux determined with the camera method is Φ_{cam}=8,37 kW and with the radiometer method Φ_{rad}=8,39 kW on the images with a maximum incident flux of about 15 kW/m² (Fig. 11 (a) and (b)). In Fig. 11 (c) and (d) the values are Φ_{cam}=19,13 kW and Φ_{rad}=18,33 kW.

CONCLUSION

We constructed and build a test receiver consisting of 16 black-coated tubes to carry out first test with this method. The results show accordance when comparing the total incident flux measured by both the camera method and the radiometer method. While the scans from higher incident angles give results that cannot be interpreted satisfyingly, we have to work on this issue to accomplish a better understanding of the process of determining the radiation reflected off the receiver. Nevertheless, the method of determining the flux map by measuring the reflection off the absorber is seen to be applicable for tube receivers. Further results with more scan directions are still in evaluation. Additional, measurements with irradiated receivers are planned in the HPMS-II (High Power Molten Salt Receiver) project at the Multi Focal Tower in Jülich and at the Ashalim Solar Thermal Power Station, Israel. This will give us the opportunity to test our system at a commercial external tube receiver during operation and is the next step towards an industrial solution for real-time flux measurements together with our project partner CSP Services.

ACKNOWLEDGMENTS

The work presented here was elaborated within the project TubeMon and was supported by the Federal Ministry for Economic Affairs and Energy on the basis of a decision by the German Bundestag and has also received funding from ERA-NET SOLAR with co-funding from CDTI and the European Union's Framework Program for Research and Innovation, Horizon 2020. Brightsource Energy, Israel, as a partner in this project, supported us with the absorbing coating for the steel tubes of the test receiver.

REFERENCES

1. Röger, M., Herrmann, P., Ulmer, S., Ebert, M., Prahl, C., Göhring, F., *Techniques to Measure Solar Flux Density Distribution on Large-Scale Receivers*, J. Sol. Energy Eng. 136(3), 031013 (10 pages), 2014, https://doi.org/10.1115/1.4027261.
2. Göhring, F., Bender, O., Röger, M., Nettlau, J., Schwarzbözl, P., *Flux Density Measurement on Open Volumetric Receivers.* Proc. of SolarPACES 2011, Sept. 20-23, Granada, Spain, 2011.
3. Offergeld, M., Röger, M., Stadler. H., Gorzalka, P., Hoffschmidt, B.: *Flux Density Measurement for Industrial-Scale Solar Power Towers Using the Reflection off the Absorber*, AIP Conference Proceedings 2126, 110002 (2019), SolarPACES, Casablanca, 2018, https://doi.org/10.1063/1.5117617
4. Offergeld, M., Röger, M., Stadler. H., *Verfahren zur Bestimmung von relativen Reflexionsgraden einer Absorberfläche eines Receivers einer Solarturmanlage*, Patent DE102016226033B4.
5. Clifford K. Ho, Siri S. Khalsa: *A Photographic Flux Mapping Method for Concentrating Solar Collectors and Receivers*, Journal of Solar Energy Engineering, Vol. 134, November 2012.